OUKA
The University of Osaka
Institutional Knowledge Archive

Title	Interplanar stiffness in defect-free monocrystalline graphite
Author(s)	Kusakabe, Koichi; Wake, Atsuki; Nagakubo, Akira et al.
Citation	Physical Review Materials. 2020, 4(4), p. 043603-1-043603-5
Version Type	VoR
URL	https://hdl.handle.net/11094/84184
rights	Copyright 2020 by the American Physical Society
Note	

The University of Osaka Institutional Knowledge Archive : OUKA

https://ir.library.osaka-u.ac.jp/

The University of Osaka

Interplanar stiffness in defect-free monocrystalline graphite

Koichi Kusakabe,[1] Atsuki Wake,[2] Akira Nagakubo,[2] Kensuke Murashima,[3] Mutsuaki Murakami,[3] Kanta Adachi,[4] and Hirotsugu Ogi[2,*]

[1]*Graduate School of Engineering Science, Osaka University, Toyonaka, Osaka 560-8531, Japan*
[2]*Graduate School of Engineering, Osaka University, Suita, Osaka 565-0871, Japan*
[3]*Material Solutions New Research Engine E & I Materials Group, Kaneka Co., Settsu, Osaka 566-0072, Japan*
[4]*Faculty of Science and Engineering, Iwate University, Morioka, Iwate 020-8551, Japan*

(Received 4 December 2019; revised manuscript received 19 March 2020; accepted 23 March 2020; published 20 April 2020)

The interplanar bond strength in graphite has been identified to be very low, owing to the contribution of the van der Waals interaction. However, in this study, we use microscopic picosecond ultrasound to demonstrate that the elastic constant, C_{33}, along the c axis of defect-free monocrystalline graphite exceeds 45 GPa, which is higher than reported values by 20%. Based on the experimental finding, we find that the LDA+U+RPA method, including both random phase approximation correlation and short-range correlation in $2p$ Wannier orbitals, can be a promising solution. The agreement of thus calculated stiffness with the observation indicates non-negligible electron correlation effects with respect to both the short-range and long-range interactions.

DOI: 10.1103/PhysRevMaterials.4.043603

The interplanar interaction between graphene sheets remains a central issue in condensed-matter physics because the participation of long-distance van der Waals interactions makes its theoretical description a labyrinth problem. A direct characteristic of an interplanar interaction is C_{33}—the elastic constant along the c axis of graphite—because it reflects the interlayer bond strength. Lechner *et al.* [1] demonstrated that C_{33} of graphite estimated by density functional theory (DFT) can range between 1.9 and 71.4 GPa, depending on the Hamiltonian basis set used. C_{33} of graphite has thus been adopted to validate proposed theoretical approaches, and its accurate measurement is critical to thoroughly understand van der Waals interactions.

As presented in Table I, previous experimental studies reported C_{33} values between 36 and 39 GPa [2–5] and recent DFT studies were conducted to yield the measured interplanar stiffness [6–8]. However, the specimens used in the studies were highly oriented graphite (HOG), not defect-free monocrystalline graphite. Due to the hexagonal symmetry about the c axis of graphite, a HOG specimen was apparently regarded as a single crystal [2]. However, grain (domain) boundaries usually deteriorate the bond strength of the material, significantly decreasing the macroscopic elastic constants. Young's moduli of nanocrystalline CaF_2, Pd, and Mg decrease by 66%, 35%, and 13%, respectively, from those of corresponding monocrystals [9] predicted by the Hill averaging method [10]. In addition, Young's moduli of nanocrystalline Pd and Cu [11], Fe [12], and Al [13] are reported to decrease by approximately 50%, 70%, 40%, and 40%, respectively. A number of other studies have been conducted on softened materials by grain boundaries. Thus, the macroscopic elastic constant of a HOG should be substantially smaller than that of monocrystalline graphite. Bosak *et al.* [5] used focused inelastic x-ray scattering to measure an area of $250 \times 60\ \mu m^2$, producing the largest C_{33} value among previous studies: 38.7 GPa. However, this size appeared too large to express the stiffness of a single grain, and experimental reports of C_{33} in defect-free monocrystalline graphite were still lacking.

In this study, we measured C_{33} of highly pure defect-free monocrystalline graphite using a microscopic picosecond-ultrasonic method. Our specimens were multilayer graphene sheets that were synthesized by heating ~3-μm-thick polyimide films at temperatures up to 2800, 3150, and 3200 °C under in-plane tension [14–16]; we refer to these sheets as G_{2800}, G_{3150}, and G_{3200}, respectively. This synthesis method allowed us to develop approximately 1.5-μm-thick highly oriented defect-free graphite specimens (Figs. 1 and 2). Figure 1 compares the Raman spectrum and the cross-section micrograph of our specimen (G_{2800}) with those of a highly oriented pyrolytic graphite (HOPG) specimen. The two materials show identical Raman spectra, suggesting that the HOPG specimen would be good enough for evaluation of the stiffness. However, its cross-section image (below) shows many domain boundaries even between c planes. On the other hand, our specimen (upper) does not involve any observable defects. The cross-section transmission-electron-micrography observation further confirmed the defect-free structures of our specimens even in nanoscale [Fig. 2(a)]. Our specimens are thus almost defect free, although the thickness is limited to be smaller than ~1.5 μm. Previous experimental methods failed to determine the out-of-plane stiffness for such a thin specimen. Our microscopic picosecond-ultrasound technique shown below, however, allows highly accurate determination of the stiffness, owing to its ultrahigh-frequency measurement.

*ogi@prec.eng.osaka-u.ac.jp

 ©2020 American Physical Society

TABLE I. Measured and calculated C_{33} in the present study and previous studies. Simulation methods are described in the main text.

		C_{33} (GPa)	Thickness (μm)	Domain size (μm)	Methods
	Present (G_{2800})	40.1 ±0.9	∼1.5	1.3	
	Present (G_{3150})	46.1 ±4.4	∼1.2	6.3	Picosecond ultrasonics
	Present (G_{3200})	48.4 ±5.3	∼1.3	8.3	
exp.	Ref. [2]	36.5	∼10, 000	–	Ultrasonic pulse echo
	Ref. [3]	36.6[a]	∼50	–	X-ray diffraction
	Ref. [4]	37.1	–	–	Inelastic neutron scattering with lattice dynamics
	Ref. [5]	38.7	∼100	–	Inelastic x-ray scattering
	Present	41 ±4	–	–	LDA+U ($U = 2.1$ [eV])
	Present	48 ±4	–	–	LDA+U+RPA ($U = 2.1$ [eV])
	Present	38	–	–	ACFDT-RPA
	Present	51 ±5	–	–	ACFDT-RPA+U ($U = 2.1$ [eV])
calc.	Ref. [6]	36	–	–	ACFDT-RPA
	Ref. [7]	33.3	–	–	vdW-DF2
	Ref. [8]	36.79	–	–	Born's long-wave method

The domain (grain) size increases as the synthesizing temperature increases, up to approximately 20 μm, as shown in Table I. Because we evaluated the domain structure using the electron-channelling contrast-imaging method, the resultant contrast like Fig. 2(b) reflects the crystallographic-orientation image, indicating that a single domain is a single crystal of graphite. Our microscopic picosecond ultrasonic method can measure the longitudinal wave velocity along the thickness direction in a localized area of approximately 1 μm in diameter, which is smaller than the domain size of the G_{3150} and G_{3200} specimens (Table I), resulting in C_{33} of the defect-free monocrystalline graphite.

The optics developed here is shown in Fig. 3. We used a titanium/sapphire pulse laser with a wavelength of 800 nm. The light pulse was split into pump and probe light pulses, and the wavelength of the probe light was converted to 400 nm. Both pulses were perpendicularly focused on the specimen surface via an objective lens. Due to the high absorption coefficient of graphite for 800-nm light, a longitudinal wave was efficiently generated without requiring any additional coating material. Figure 3 also presents an irradiation image, in which a measurement spot of approximately 1.5 μm in diameter is indicated.

Figure 4(a) illustrates the typical reflectivity change and the inset presents the baseline subtracted reflectivity. We were able to clearly observe the pulse-echo signals of the longitudinal wave propagating along the thickness direction, from which we determined the round-trip time and elastic constant C_{33} using the mass density, 2260 kg/m^3, and the specimen thickness, which is a key parameter for determining the elastic constant. After the picosecond ultrasonic measurement, we lifted a small slice of the specimen near the surface using a

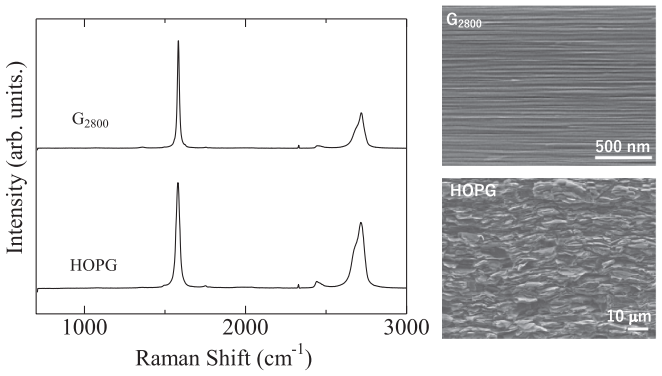

FIG. 1. Comparison of Raman spectrum and cross-section microstructure observed by scanning-electron micrography of our specimen (G_{2800}) (upper) with those of a highly oriented pyrolytic graphite (lower).

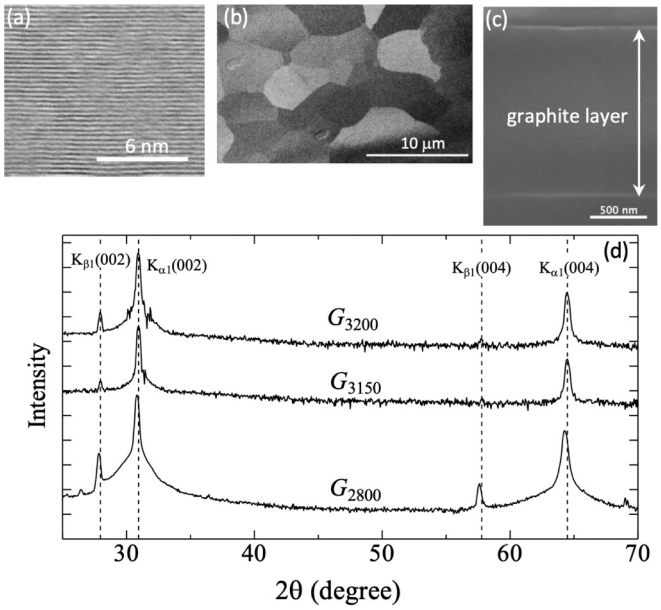

FIG. 2. (a) Cross-section transmission electron microscopy image for specimen G_{2800}; (b) in-plane electron-channelling-contrast image for specimen G_{3200}; (c) cross-section scanning electron microscopy image for specimen G_{3200}; (d) x-ray diffraction spectra of three graphite specimens (Co target). The vertical axis shows the logarithmic intensity. The average c-axis lattice parameter was 6.712 Å.

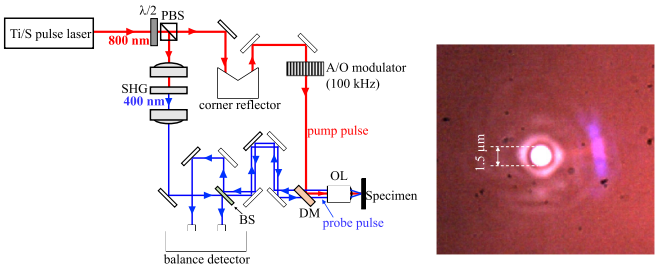

FIG. 3. Microscopic picosecond ultrasound optics (left) and an irradiation image on a gauged specimen with microscopic picosecond ultrasound (right).

focused ion beam processing technique, which is widely used to prepare a specimen for transmission electron microscopy for cross-sectional observation. We observed its cross-section by electron microscopy, as illustrated in Fig. 2(c). Figure 4(b) presents a line scan of the elastic constant. The C_{33} value is generally within 45–50 GPa; however, it is occasionally significantly smaller. We consider these softened regions to correspond to measurements near the domain boundary, where possible factors to lower the effective stiffness will densely appear, including voids, lattice defects, and low crystallinity region. Because the measurement region in this study is of the order of 1 μm, which is much smaller than those in previous studies, such factors can be enhanced compared with the previous macroscopic measurements. As shown in Table I, the error for the elastic-constant determination (or the stiffness fluctuation on the specimen surface) becomes smallest for the G_{2800} specimen, which exhibits the domain size close to the measurement region, indicating that each measurement point contains a certain level of the softened region. The observation that the average stiffness and the stiffness fluctuation decrease as the domain size becomes smaller supports our view that the stiffness will be lowered near the domain boundary.

Recent DFT calculations [6–8] yield smaller C_{33} values than our experiments. For example, we used the adiabatic-connection fluctuation-dissipation-theorem with random-phase approximation (ACFDT-RPA) calculation following Lebégue *et al.* [6] and confirmed that the deduced C_{33} value could not exceed 39 GPa, as illustrated in Table I [17]. Such a discrepancy between theory and experiment is also found in the binding energy along the c axis. The binding energy calculated by the previous theory [6] is smaller than that yielded by a recent high-quality experiment [18] by 12%. Because positive correlation between the binding energy and C_{33} is expected, C_{33} of graphite should be significantly higher than the previous calculations. Another clue was found when a little overbinding property was concluded in interlayer distance d. By both RPA and LDA (at $U = 0$), d was estimated about 1% shorter than the observed value of $d_{\rm exp}$. The determined value of $d/d_{\rm exp}$ is given in Table II, where $d_{\rm exp} = 3.356$ Å.

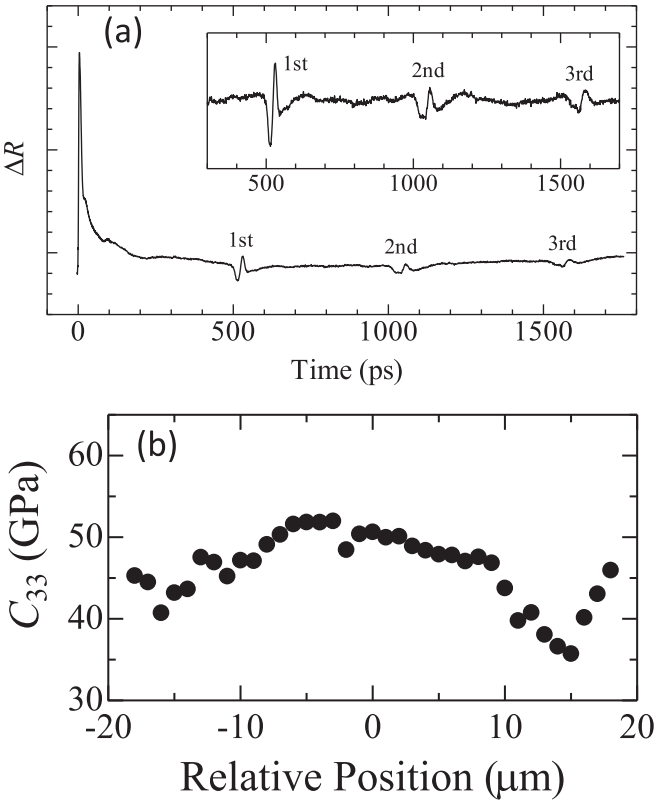

FIG. 4. (a) Reflectivity change measured using the microscopic picosecond ultrasonic method for G_{3150}; (b) one-dimensional elastic-constant distribution on the specimen.

To amend the shortened d and the small value of C_{33}, we here propose a perturbation method coupled with the estimation of correlation effects in both long- and short-range schemes. This method improves the DFT local density approximation (DFT-LDA) calculation for both C_{33} and the lattice constant of graphite, providing a larger d and an increased C_{33} than LDA simultaneously. In Supplemental Material A, we introduce two schemes [19]. Starting from the LDA+U total energy, we substitute the LDA correlation with the ACFDT-RPA correlation, which is called LDA+U+RPA. We can also introduce residual short-range correlation, the Hubbard correlation energy, into the ACFDT-RPA calculation (ACFDT-RPA+U). For the LDA+U calculation, we adopt a scheme using a Wannier orbital with the double-counting correction [20]. The Wannier orbitals with p symmetry on each carbon were determined at each point on the Born-Oppenheimer potential energy surface (PES).

Dependence of the calculational interlayer distance d on U is shown in Fig. 5. In LDA+U, by introducing nonzero U, d started to increase and went through $d_{\rm exp}$. The rate of increase was a little reduced in LDA+U+RPA and ACFDT-RPA+U.

TABLE II. Estimated interlayer distance $d/d_{\rm exp}$ determined by simulation methods. $d_{\rm exp} = 3.356$ [Å] is the observed value in the experiment. In LDA+U, LDA+U+RPA, and ACFDT-RPA+U, the value of U is approximated by 2.1 ±0.5 [eV].

Method	LDA	ACFDT	LDA+U	LDA+U+RPA	ACFDT-RPA+U
	0.990 ± 0.002	0.991 ± 0.001	1.030 ± 0.006	1.021 ± 0.005	1.021 ± 0.005

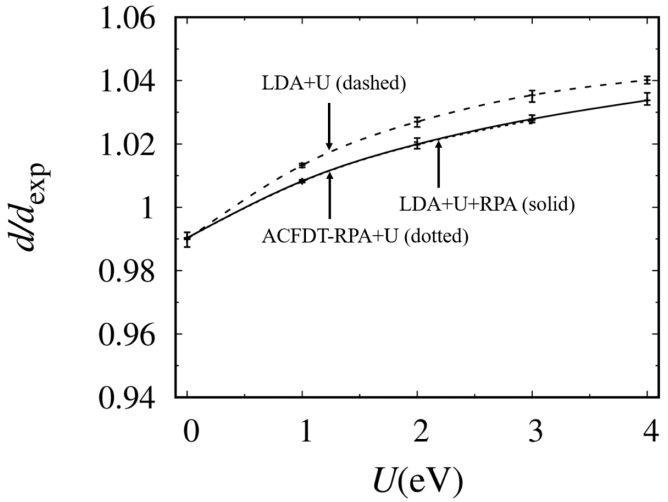

FIG. 5. Optimized interplane distance d by LDA+U (dashed curve), LDA+U+RPA (solid curve), and ACFDT-RPA+U (dotted curve), relative to the experimentally observed value of $d_{exp} = 3.356$ Å.

Both of these simulation methods produced rather large corrections of C_{33}. Adopting k meshs from $32 \times 32 \times 16$ to $44 \times 44 \times 22$, we find reasonable convergence in estimated C_{33} as shown in Fig. 6. Enhancement of C_{33} from the value by ACFDT-RPA comes from nonharmonic contribution of the U term. The self-consistently determined $2p$ Wannier orbitals at each value of d is key for the correction, which is a kind of renormalization in the wave function. Owing to the short-range correlation effect, PES becomes selectively enhanced in a range of $d < d_{exp}$. Relative to the LDA result, replacement of the exchange-correlation energy by RPA correlation and the exact exchange causes deepened PES. Both short-range

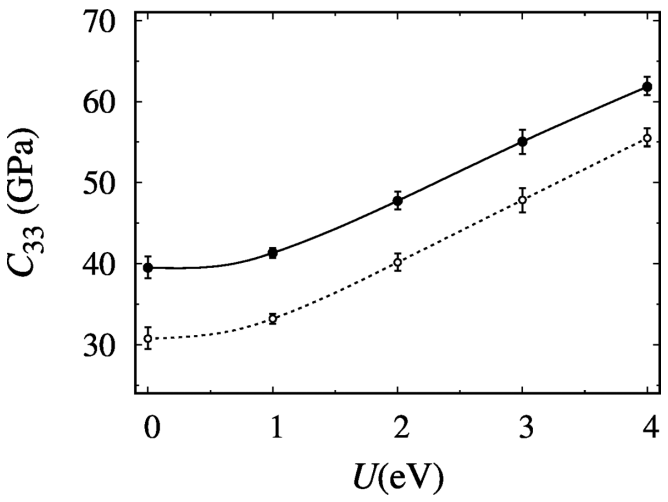

FIG. 6. Calculated C_{33} by LDA+U with and without RPA correction. The horizontal axis denotes the strength of U [eV]. Closed (open) circles are given by LDA+U with (without) RPA correction. The vertical bar at each point denotes a range of the estimated C_{33} by several k-mesh points from $14 \times 14 \times 6$ to $44 \times 44 \times 22$ points. Constrained RPA (cRPA) estimation results in an estimated value of $U \sim 2.1 \pm 0.5$ [eV] for a Wannier orbital with p_z symmetry.

(+U) and long-range (RPA) correlations cause enhancement of C_{33}.

Our scheme of multireference DFT [21–23] allows determination of U in the same formalism. The theoretical background [24–43] is provided in Supplemental Material A [19]. As an approximation, a constrained RPA (cRPA) evaluation of U is applicable. The on-site U showed a non-negligible contribution. When we adopt $U \simeq 2.1 \pm 0.5$ eV by cRPA, we have $C_{33} \simeq 48 \pm 4$ GPa. In this LDA+U+RPA, however, the estimated d becomes 2% larger than d_{exp} (Table II). Simultaneous reproduction of d and C_{33} in a perfect manner was not found on a single axis of U. However, this simple method, which is accessible within a computational timescale comparable to ACFDT-RPA and cRPA, certainly provides a vision that inclusion of two kinds of correlation effects can efficiently allow us approach the tendency of PES found in a former quantum Monte Carlo simulation [44].

Upon adding the Hubbard correction, using the self-consistent calculation by LDA for the ACFDT-RPA+U calculation, we obtain an ever larger C_{33} of approximately 51 ± 5 GPa in ACFDT-RPA+U. This approximation, however, may contain an overestimation error because the wave function adopted for the +U correction is not used for the mean-field ground-state energy containing kinetic and electron-ion energy contributions. Further consideration of middle-range correlation, e.g., multiple correlation terms as further corrections, is left as a future work.

In the above estimation, the value of U in cRPA is assumed to be independent of the c-axis lattice parameter, c. In fact, there exists a linearly dependent shift in U around the equilibrium structure, whereby a smaller c leads to a larger U in cRPA. Then, the total energy curve is shifted by a linear contribution from the Hubbard term and the double-counting correction term. Although this effect can lead to an increased c, C_{33}, as the second-order derivative of the total energy E_{tot} with respect to c, is not affected by the correction linear to U. The correction stems from λ integration with respect to the difference between the Hubbard terms, that is, the Hubbard interaction and the double-counting correction, and their mean-field approximations. By applying a constant U approximation, however, we obtain a reasonable result for the estimated volume within an accuracy of several percent.

In summary, we use a microscopic picosecond ultrasound measurement to demonstrate that defect-free monocrystalline graphite exhibits a C_{33} value above 45 GPa, which exceeds the value estimated by ACFDT-RPA. Considering the short-range correlation effect, the theoretical estimation of C_{33} can produce a value larger than 45 GPa, as exemplified by our proposed LDA+U + RPA or ACFDT-RPA+U methods.

ACKNOWLEDGMENTS

This study is supported by JSPS KAKENHI Grants No. JP19H00862 and No. JP18K03456. The calculations were done in the computer centers of Kyushu University and ISSP, University of Tokyo.

ATTRIBUTIONS

K.K. performed theoretical estimation of C_{33} with MR-DFT and wrote the paper. A.W. and A.N. performed the picosecond ultrasonics measurements. K.M. and M.M. synthesized the defect-free graphite specimens. K.A. contributed to development of the optics. H.O. produced this study, performed the picosecond ultrasonics measurements, analyzed specimens, and wrote the paper.

[1] C. Lechner, B. Pannier, P. Baranek, N. C. Forero-Martinez, and H. Vach, J. Phys. Chem. C **120**, 5083 (2016).
[2] O. L. Blakslee, D. G. Proctor, E. J. Seldin, G. B. Spence, and T. Weng, J. Appl. Phys. **41**, 3373 (1970).
[3] N. Wada, R. Clarke, and S. A. Solin, Solid State Commun. **35**, 675 (1980).
[4] R. Nicklow, N. Wakabayashi, and H. G. Smith, Phys. Rev. B **5**, 4951 (1972).
[5] A. Bosak, M. Krisch, M. Mohr, J. Maultzsch, and C. Thomsen, Phys. Rev. B **75**, 153408 (2007).
[6] S. Lebégue, J. Harl, Tim Gould, J. G. Ángyán, G. Kresse, and J. F. Dobson, Phys. Rev. Lett. **105**, 196401 (2010).
[7] I. V. Lebedeva, A. V. Lebedev, A. M. Popov, and A. A. Knizhnik, Comput. Mater. Sci. **128**, 45 (2017).
[8] K. H. Michel and B. Verberck, Phys. Rev. B **78**, 085424 (2008).
[9] D. Korn, A. Morsch, R. Birringer, W. Arnold, and H. Gleiter, J. Phys. (Paris) **49**, C5-769 (1988).
[10] R. Hill, Proc. Phys. Soc. A **65**, 349 (1952).
[11] G. W. Nieman, R. J. Weertman, and R. W. Siegel, J. Mater. Res. **6**, 1012 (1991).
[12] E. Bonetti, E. G. Campari, L. D. Bianco, and G. Skipione, Nanostructured Mater. **6**, 639 (1995).
[13] T.-Y. Zhang, and J. E. Hack, Phys. Status Solidi A **131**, 437 (1992).
[14] J. Sone, M. Murakami, and A. Tatami, Micromachines **9**, 64 (2018).
[15] M. Murakami, A. Tatami, and M. Tachibana, Carbon **145**, 23 (2019).
[16] H. Mogi, T. Bamba, M. Murakami, Y. Kawashima, M. Yoshimura, A. Taninaka, S. Yoshida, O. Takeuchi, H. Oigawa, and H. Shigekawa, ACS Appl. Electron. Mater. **1**, 1762 (2019).
[17] We used a parameter set similar to the literature [6].
[18] W. Wang, S. Dai, X. Li, J. Yang, D. J. Srolovitz, and Q. Zheng, Nat. Commun. **6**, 7853 (2015).
[19] See Supplemental Material at http://link.aps.org/supplemental/10.1103/PhysRevMaterials.4.043603 for details on theoretical background and computation.
[20] M. Cococcioni and S. de Gironcoli, Phys. Rev. B **71**, 035105 (2005).
[21] K. Kusakabe, J. Phys. Soc. Jpn. **70**, 2038 (2001).
[22] K. Kusakabe, N. Suzuki, S. Yamanaka, and K. Yamaguchi, J. Phys.: Condens. Matter **19**, 445009 (2007).
[23] K. Kusakabe and I. Maruyama, J. Phys. A: Math. Theor. **44**, 135305 (2011).
[24] D. C. Langreth and J. P. Perdew, Phys. Rev. B **15**, 2884 (1977).
[25] N. Hadjisavvas and A. Theophilou, Phys. Rev. A **30**, 2183 (1984).
[26] A. M. Rappe, K. M. Rabe, E. Kaxiras, and J. D. Joannopoulos, Phys. Rev. B **41**, 1227(R) (1990).
[27] V. I. Anisimov, J. Zaanen, and O. K. Andersen, Phys. Rev. B **44**, 943 (1991).
[28] V. I. Anisimov, I. V. Solovyev, M. A. Korotin, M. T. Czyźyk, and G. A. Sawatzky, Phys. Rev. B **48**, 16929 (1993).
[29] G. Kresse and J. Hafner, Phys. Rev. B **47**, 558 (1993).
[30] G. Kresse and J. Furthmüller, Phys. Rev. B **54**, 11169 (1996).
[31] G. Kresse and J. Furthmüller, Comput. Mater. Sci. **6**, 15 (1996).
[32] I. V. Solovyev, P. H. Dederichs, and V. I. Anisimov, Phys. Rev. B **50**, 16861 (1994).
[33] Y. M. Niquet, M. Fuchs, and X. Gonze, Phys. Rev. A **68**, 032507 (2003).
[34] T. Fujiwara, S. Yamamoto, and Y. Ishii, J. Phys. Soc. Jpn. **72**, 777 (2003).
[35] F. Aryasetiawan, M. Imada, A. Georges, G. Kotliar, S. Biermann, and A. I. Lichtenstein, Phys. Rev. B **70**, 195104 (2004).
[36] K. Nakamura, R. Arita, and M. Imada, J. Phys. Soc. Jpn. **77**, 093711 (2008).
[37] Y. Kanai and J. C. Grossman, Phys Rev. A **80**, 032504 (2009).
[38] P. Giannozzi, S. Baroni, N. Bonini, M. Calandra, R. Car, C. Cavazzoni, D. Ceresoli, G. L. Chiarotti, M. Cococcioni, I. Dabo, A. Dal Corso, S. de Gironcoli, S. Fabris, G. Fratesi, R. Gebauer, U. Gerstmann, C. Gougoussis, A. Kokalj, M. Lazzeri, L. Martin-Samos, N. Marzari, F. Mauri, R. Mazzarello, S. Paolini, A. Pasquarello, L. Paulatto, C. Sbraccia, S. Scandolo, G. Sclauzero, A. P. Seitsonen, A. Smogunov, P. Umari, and R. M. Wentzcovitch, J. Phys.: Condens. Matter **21**, 395502 (2009).
[39] K. Nakamura, Y. Yoshimoto, T. Kosugi, R. Arita, and M. Imada, J. Phys. Soc. Jpn. **78**, 083710 (2009).
[40] Y. Nohara, S. Yamamoto, and T. Fujiwara, Phys. Rev. B **79**, 195110 (2009).
[41] T. Olsen and K. S. Thygesen, Phys. Rev. B **87**, 075111 (2013).
[42] K. Nakamura, Y. Nohara, Y. Yosimoto, and Y. Nomura, Phys. Rev. B **93**, 085124 (2016).
[43] T. Olsen, C. E. Patrick, J. E. Bates, A. Ruzsinszky, and K. S. Thygesen, npj Comp. Mater. **5**, 106 (2019).
[44] L. Spanu, S. Sorella, and G. Galli, Phys. Rev. Lett. **103**, 196401 (2009).